

## **Trace and rare earth element systematics of cold-seep carbonates from the Krishna-Godavari basin: A comparison between isotopically distinct carbonate deposits.**

**Muralidhar Kocherla<sup>1\*</sup>, Durbar Ray<sup>1</sup>, M. Satyanarayanan<sup>2</sup>, H.M. João, Christo Sojan<sup>1</sup>**

<sup>1</sup>CSIR-National Institute of Oceanography, Dona Paula, Goa- 403004, India.

<sup>2</sup>CSIR-National Geophysical Research Institute, Uppal Road, Hyderabad- 500007, India.

\*Corresponding author: Muralidhar Kocherla, CSIR-National Institute of Oceanography, Dona Paula, Goa- 403004. Email: [kocherla@nio.org](mailto:kocherla@nio.org)

### **Abstract**

Mineralogical and isotopically distinct authigenic carbonates from the zones of methane oxidation and methanogenesis in the cold-seep environment, from the Krishna-Godavari basin are investigated for major, trace, and rare earth element compositions. For this study, the elemental compositions of the <sup>13</sup>C-depleted carbonate phase ( $\delta^{13}\text{C} < -45\%$ ) developed under the influence of anaerobic methane oxidation in the shallow parts (<115mbfs) of a sediment core, are compared with those in isotopically heavier siderite ( $\delta^{13}\text{C} > +5\%$ ) from the zone of microbial methanogenesis at the deeper sediment depths (115-197mbfs). Results showed both types of cold-seep carbonate in two geochemical regimes have a comparable range of concentrations of redox-sensitive (e.g. V, Cr, Co, Ni, Zn) and refractory elements (e.g. Sc, Cs, Ga, Zr, Hf, Ta, Th), indicating limited impacts of mineralogy and their genetic processes on the distribution of these elements. In contrast, the degree of enrichments of elements like Si, Al, Sr, Y, HREE, and U in those isotopically discrete seep carbonates were distinctly different. Such compositional variability in two types of authigenic carbonates is described in terms of their diverse formation mechanisms, mineralogical controls, and variable contributions of terrigenous materials.

**Keywords:** Bay of Bengal; K-G basin; Authigenic carbonates; Trace elements; Rare Earth elements.

## 1. Introduction

Globally, numerous reports document the occurrence of authigenic carbonates in sedimentary columns, along the continental margins, often associated with significant methane seepage (Hovland et al., 1987; Han and Suess, 1989; von Rad et al., 1996; Teichert et al., 2005; Mazzini et al., 2006). These sedimentary authigenic carbonates not only serve as evidence of ongoing methane seepage activity, but they are also indicative of paleo-seepage activities (Mazumdar et al., 2009; Peckmann et al., 2009). In the northern Bay of Bengal, occurrences of methane-derived authigenic carbonates have been reported from the Krishna-Godavari basin (K-G basin) along the Eastern continental margins of India (Kocherla et al., 2006; Mazumdar et al., 2009). The widespread presence of gas hydrates has been confirmed through multi-channel seismic observations. Geochemical analyses of long sediment piston cores (~200m), drilled during the National Gas Hydrate Program (NGHP-01) expedition in 2006, have further validated the existence of massive authigenic carbonate concretions (Collett et al., 2008, Teichert et al., 2014, Kocherla et al., 2015; Gaikwad et al., 2021). These cores also revealed the occurrence of thick gas hydrate layers (more than 100m) within the sediment columns in the KG- basin (Kocherla et al., 2006, Ramana et al., 2007, Collett et al., 2008, Mazumdar et al., 2009, Dewangan et al., 2010).

Other geophysical evidence including the slumping/sliding of slope sediments, and the development of several bathymetric mounds suggesting high and erratic sedimentation rates, which further substantiate the fluid and/or gas migration through the fault system within the K-G basin (Dewangan et al., 2010, Ramprasad et al., 2011). Several studies have described the geochemical characteristics of the methane-hydrates and associated sediments and thus discussed several issues related to the genesis of hydrates (Teichert et al., 2014; Solomon et al., 2014; Kocherla et al., 2015). To date, the source of methane and the details of sub-surface processes involved in the genesis of methane-seep carbonates in the K-G basin have been discussed by several authors (Kocherla et al., 2006; Mazumdar et al., 2009; Teichert et al., 2014). However, information on the elemental compositions of these carbonate concretions is rare. Particularly, the impacts of different geochemical processes on the abundances of trace and rare earth elements in these cold-seep carbonates have sparsely been discussed in previous studies.

In the present study, we provide a comprehensive analysis of the major, trace, and rare earth element compositions of authigenic carbonates associated with cold seeps in the K-G basin. Specifically, we delve into the elemental compositions of prevalent carbonates from two distinct geochemical settings across various depth regimes, which have been discussed in light of their modes of formation. Moreover, leveraging trace element systematics, we aim to elucidate the likely

nature of the source fluids that played a role in the genesis of these cold-seep carbonates.

## **2. Local geological settings**

The K-G basin (Fig. 1) is described as a peri-cratonic, passive rift basin located at the central part of the eastern continental margins of India (Rao, 2001). Around 130Ma years ago, this marginal basin evolved after the breakup of Gondwanaland (Scotese et al., 1988; Ramana et al., 1994). The onshore extension of this basin has an area of ~28,000 km<sup>2</sup>, while its off-shore coverage in the northern Bay of Bengal occupies an area of 1.45x10<sup>5</sup> km<sup>2</sup> (Ojha and Dubey, 2006). This marginal basin comprises a wide variety of geologic settings, including river deltas, coastal basins, shelf-slope aprons, deep-sea channels, and fan complexes. Most of the parts of this marginal basin are covered with silty-clay-type fine sediments (Kocherla et al., 2006; 2015; Teichert et al., 2014). The clay fraction is mostly composed of montmorillonite with traces of illite and kaolinite. The sediment thickness in near-shore areas mostly varies from 3 to 5 km while that increases further up to about 8 km towards offshore regions (Prabhakar and Zutshi, 1993). Previous studies also indicated that the sedimentary columns are characterized by several cycles of deposition, ranging from early Cretaceous to Holocene time (Rao, 2001). Besides coastal erosions, the fluvial fluxes through the major river systems of Krishna and Godavari also contribute a variety of detrital materials in this marginal basin. Based on high-resolution seismic, sub-bottom profiler (SBP), and multi-beam bathymetric surveys, various depositional environments, including mid-slope mini basins, bathymetric mounds, toe-thrust sedimentary ridges, and deep oceanic basin were identified around this study area (Ramana et al., 2007, 2009; Dewangan et al., 2010; Ramprasad et al., 2011). The acoustic observations and geochemical analyses of sediment have confirmed the evidence of widespread migration of gas and the substantial presence of gas hydrate in the sediment core (Ramana et al., 2007; Mazumdar et al., 2009; Dewangan et al., 2010).

## **3. Collection of samples and analytical methods**

During the first expedition of the Indian National Gas Hydrate Program (NGHP-01) onboard *D/V JOIDES RESOLUTION* in 2006, several sediment cores were drilled out from the K-G basin (Dewangan et al., 2010; Ramprasad et al., 2011). At the designated site, NGHP-01-10D (15°51.8'N; 81°50.1'E, Fig. 1), a 203.8m long core was collected from the water depth of 1040 m. This core contained several thick gas-hydrate bearing layers between 29 and 157 mbsf (Collett et al., 2008; Lee and Collett, 2009), and methane-related carbonate deposits at multiple depths between 6 and 197 mbsf. In the laboratory, a total of 32 carbonate concretions were isolated from the sediments of

eight different core depths (Table 1). These carbonate concretions were thoroughly cleaned with Milli-Q water, involving immersion in an ultrasonic bath, followed by air drying. Subsequently, the dried carbonate concretions were investigated for physical features, mineralogy, inorganic carbon contents, carbon and oxygen isotope ratios, and major, trace, and rare earth element compositions.

### ***3.1. Microscopic observation and mineralogy***

The carbonate concretions from different depths of the NGHP-01-10D core were thoroughly examined for size, morphology, and other external features using a Nikon® SMZ-1500 microscope. For a detailed visualization of surface texture and crystal habits, these carbonate concretions were examined with a JEOL-JSM® 5800 LV1 electron microscope. Additionally, dry powdered samples (n=8) of those carbonates were analyzed for mineralogy with an X-ray diffractometer (Rigaku Ultima®-IV) over the  $2\theta$  ranges from  $20^\circ$  to  $55^\circ$  at the rate of  $1.0^\circ/\text{min}$ , using Cu-K $\alpha$  radiation. The shifts in the d (104) carbonate peaks were used to determine the Mg-contents of calcite concretions (Lumsden, 1979).

### ***3.2. Total inorganic carbon contents and carbon isotopic compositions***

The total inorganic carbon (TIC) contents in the carbonate samples were determined using a coulometer (UIC Model 5130). In this process, approximately 30 mg of dried sample was acidified with 2N HCl and heated in a vial to generate CO<sub>2</sub>. Subsequently, the generated CO<sub>2</sub> was allowed to pass through the scrubbing system of the coulometer for quantitative estimation; using extra pure calcium carbonate as the external standard.

The stable carbon and oxygen isotopic compositions of carbonate concretions were determined with a continuous flow Isotope Ratio Mass Spectrometer (Thermo Finnigan Delta plus® XP) coupled with a GASBENCH-II gas preparation and induction system, following the method described by Kocherla et al. (2015). For this dry powdered samples were treated with phosphoric acid and then the CO<sub>2</sub> generated in the reaction was analysed with a dual collector IRMS. The isotopic compositions are reported in terms of “ $\delta$ ” notation relative to the *Vienna Peedee belemnite* (VPDB) standard. For both  $\delta^{13}\text{C}_{\text{VPDB}}$  and  $\delta^{18}\text{O}$  measurements, an analytical precision of 0.1‰, while the analytical accuracy was  $\pm 0.06\text{‰}$  for  $\delta^{13}\text{C}$  and  $\pm 0.04\text{‰}$  for  $\delta^{18}\text{O}$  measurements, respectively.

### ***3.3. Elemental composition***

The major element composition of carbonate concretions was determined by using dry powdered samples with an X-ray fluorescence spectrometer (PANalytical PW-2440 Magix-PRO®),

Netherlands). To analyze trace elements associated with carbonate fractions, a selective chemical leaching method (e.g. Yang et al., 2022) was followed before elemental analyses. In this method, 50 mg of finely powdered sample was weighed in 100 ml centrifuge tubes. The samples were then treated with 40 ml of 5% supra pure acetic acid and then kept on a vertical shaker for 16 hours, and then subsequently centrifuged at 3000 rpm for 15 minutes. This procedure ensured the complete extraction of the carbonate fraction with negligible or minimal contribution from the non-silicates. Subsequently, 5 ml of 1.0 ng/ml  $^{103}\text{Rh}$  solution was added as internal standard and the final volume was made up to 250 ml with Milli-Q water. In these solutions, trace and rare earth element concentrations were analyzed with a quadrupole ICP-MS ((Perkin–Elmer SCIEX ELAN<sup>®</sup> DRC-II) using JLS-1 and JDo-1 as the reference standards from the Geological Survey of Japan. The necessary corrections for isobaric interferences (Balaram and Rao, 2003) were applied to obtain the actual concentration of elements. An accuracy of approximately ~2.0% was achieved against the reference standards, and the analytical precision was better than  $\pm 4.0\%$ .

#### **4. Results and discussion**

Preliminary observations on the sediment core (NGHP-01-10D) reveal a predominant composition of nanofossil-bearing silt and clay, along with noticeable gas-hydrate dissociation features. Within this core, a distinct sulfate-methane transition zone (SMTZ) was identified at an approximate depth of ~17.2 mbsf, while the gas hydrate stability zone (GHSZ) extended beneath 29 mbsf, as reported in the NGHP-01 Expedition Report. Significantly, both above and below the SMTZ, there were conspicuous occurrences of hydrate-associated carbonates at various core depths (Fig. 2). Fig. 3 presents a representation of dominant carbonate types extracted from this core.

##### ***4.1. Down-core distribution of authigenic carbonates: Variations of mineralogy, petrography, and carbon isotopic compositions***

The carbonate concretions retrieved from the upper part of the core (specifically Unit-I and Unit-IIa between 0-115 mbsf, as depicted in Fig. 2) exhibited high Lithification and were primarily composed of calcites with traces of cerussite, witherite, strontianite, aragonite, and quartz, etc. These calcite concretions displayed nodular, tubular, and crust-like textures, having size ranges between 0.2 and 2 cm (Fig. 3). The petrographic observations on the thin sections of these calcite concretions depict typical micritic texture with several veins and fissures-like features (Fig. 4).

In the deeper sections of the core, moderately lithified, yellowish-colored, nodular Fe-rich carbonates (siderite) were predominant within 115-200 mbsf range (i.e., Unit-IIb and Unit-III, in Fig.

2). In gas hydrate-bearing cores, within the zone of methanogenesis involving the reduction of sedimentary Fe-oxyhydroxides, a substantial amount of dissolved  $\text{Fe}^{2+}$  is generated, forming ferrous oxides in a reducing environment. This reacts with residual dissolved  $\text{CO}_2$ /carbonates in pore water (Rodriguez et al., 2000; Teichert et al., 2014), facilitating the mineralization of siderite. The mineralogy of these siderite concretions revealed a minor presence of cerussite, witherite, quartz, and feldspar (Table 1). Mineralogy of those siderite-concretions showed the trivial presence of cerussite, witherite, quartz, and feldspar (Table 1).

Microscopic observations of siderite displayed rounded, sub-angular, and intraclastic textures with sizes ranging from 0.1 to 0.9 cm (Fig. 3). Many siderite concretions were found to contain mussel-shell fragments within their structure, with some also preserving foraminiferal tests, occasionally filled with pyrite framboids (Fig. 5). SEM observations indicated that siderite possessed euhedral microcrystalline structures with numerous vesicles (Fig. 4), resembling other cold-seep-driven carbonate deposits reported elsewhere (Peckmann and Thiel, 2004; Teichert et al., 2005; Naehr et al., 2007). This down-core carbonate distribution with shallow calcite and deep siderite horizons closely resembled patterns reported in hydrate-bearing sedimentary columns in the Blake Ridge off the Carolina coast (Rodriguez et al., 2000).

The Total Inorganic Carbon (TIC) contents in both types of carbonate concretions exhibit similar values, ranging from 8.7 to 9.2% in calcites and 7.8 to 9.2% in siderites (Table 1). However, these carbonates display distinct carbon isotopic ratios. The enrichment in  $^{12}\text{C}$  in calcite samples ( $\delta^{13}\text{C} = -52$  to  $-43\text{‰}$ ) differs significantly from the  $^{13}\text{C}$ -rich compositions ( $\delta^{13}\text{C} = +4.9$  to  $+10.2\text{‰}$ ) observed in siderites, particularly those developed at deeper horizons (Table 1). These contrasting isotopic signatures indicate diverse carbon sources and precipitation mechanisms were involved in their formations.

The depleted  $^{13}\text{C}$  values of calcite are comparable to those ( $\delta^{13}\text{C} = -60$  to  $-27\text{‰}$ ) reported in many other cold-seep carbonate deposits (e.g., Feng et al., 2009a; Bojanowski et al., 2015; Ruban et al., 2020; Yang et al., 2022) but lighter than typical marine carbonates ( $\delta^{13}\text{C} = -0.8$  to  $+1.2\text{‰}$ , Degens and Epstein, 1964). Earlier studies suggest that in shallow cold-seep environments, the lighter C-isotope-rich calcite could develop through anaerobic oxidation of methane (AOM), originating from the dissociation of gas hydrate in deeper sediment (Roberts et al., 1993; Suess et al., 1999; Hinrichs et al., 1999; Greinert et al., 2001; Naehr et al., 2007; Feng et al., 2009a; Peckmann et al., 2009).

In contrast, the heavier C-isotopic composition of siderite in deeper sediment may result from precipitation mechanisms other than anaerobic methane oxidation. Such authigenic Fe-rich

carbonates could originate as by-products of methanogenesis mediated through microbial processes (Mozley and Carothers, 1992; Boetius et al., 2000; Kocherla et al., 2015).

Studies by Teichert et al. (2014) indicate that during methanogenesis, residual dissolved inorganic carbon (DIC) in pore water becomes depleted in lighter C-isotopes, and carbonates originating through CO<sub>2</sub> neutralization become enriched with heavier C-isotopes. Pore-water studies at the NGHP-01-10D site have shown enrichment of <sup>13</sup>C in DIC ( $\delta^{13}\text{CDIC} = 0.0$  to  $+10\text{‰}$ ) below the SMTZ (Solomon et al., 2014). Even at deeper depths ( $>120\text{mbsf}$ ) of the same core, the  $\delta^{13}\text{CDIC}$  values were found to vary within the range of  $+10$  to  $+12\text{‰}$  (unpublished data). Thus, the comparable <sup>13</sup>C-rich composition of siderite and DIC in pore water confirms that DIC originating through methanogenesis has a direct contribution to Fe-carbonate precipitation in the deeper parts of the sediment core.

Despite the distinct modes of formation leading to the development of High-Mg calcite and siderite concretions through different carbon sources, their oxygen-isotope compositions ( $\delta^{18}\text{O}$ ) exhibit a very narrow range between  $+4.1$  and  $+4.8\text{‰}$  (Table 1). These estimated  $\delta^{18}\text{O}$  values are comparable to those reported in many other hydrate-associated carbonate deposits elsewhere ( $\delta^{18}\text{O} = +2.0$  to  $+7.0\text{‰}$ ; Roberts et al., 2010; Bojanowski et al., 2015) but significantly differ from typical marine limestone ( $\delta^{18}\text{O} < -3.0\text{‰}$ ; Zhao and Zheng, 2014; Yang et al., 2021).

Generally, the oxygen-isotopic composition in cold seep carbonates reflects isotope fractionation in the source fluid, predominantly influenced by its evolution, including the temperature of formation and/or sources of oxygen (Aloisi et al., 2000; Naehr et al., 2007). However, the temperature factor is deemed unlikely because the observed  $\delta^{18}\text{O}$  values are only feasible at extremely low temperatures of the source fluid, potentially even below the freezing point of water. Therefore, the mixing of isotopically heavier water, resulting from the dissociation of methane hydrates in the sedimentary column (Hesse, 2003; Roberts et al., 2010; Bojanowski et al., 2015), might be responsible for the enrichment of heavy oxygen isotopes in both types of seep carbonate.

#### ***4.2. Major oxides and trace element compositions of calcite and siderite: Constraints on the nature of source fluids and geochemical processes***

The major oxides analyses of calcite concretions from four shallow sedimentary depths ( $<115\text{mbsf}$ ) reveal an almost uniform composition, with 39-40% CaO, 5-6% MgO, 2-2.5% Fe<sub>2</sub>O<sub>3</sub>, and 0.02-0.15% MnO (Table 2). The average Mg content in all these calcite concretions is approximately 5.4 wt%, corresponding to  $\sim 13.6\text{ mol\%}$  of MgCO<sub>3</sub>. Calcite deposits with 5-20 mol% MgCO<sub>3</sub> are commonly categorized as high-magnesium calcite (HMC), as described elsewhere (Bayon et al.,

2007, Novikova et al., 2015, Yang et al., 2022). Previous studies have suggested that in gas-hydrate-associated carbonate deposits, HMC develops from low-temperature pore fluid with high dissolved Mg/Ca ratios, typically near the sulfate reduction zone of any sedimentary column (Bayon et al., 2007, Gieskes et al., 2005).

In these HMC concretions, substantial amounts of SiO<sub>2</sub> (10.7-12%), Al<sub>2</sub>O<sub>3</sub> (2.9-3.4%), TiO<sub>2</sub> (0.21-0.27%) (see Table 2) and their strong correlations ( $r = 0.78-0.99$ ) indicate a significant contribution of terrigenous materials into these shallow authigenic deposits. In comparison to HMC, the siderite concretions at deeper horizons (>115 mbsf) within the zone of methanogenesis in the sediment column exhibit lower SiO<sub>2</sub> (4.8-8.9%), Al<sub>2</sub>O<sub>3</sub> (0.8-2.3%), and TiO<sub>2</sub> (0.18-0.37%) contents (Table 2), indicating a relatively lower contribution of detrital minerals. However, in the deep horizons, such Fe-mineralization (with 38-49% Fe<sub>2</sub>O<sub>3</sub>, Table 2) confirms the involvement of Fe-rich source fluid during authigenic carbonate precipitation. In deeper layers of the core, the genesis of methane typically involves diagenetic changes, including the reduction of sedimentary metal oxides, particularly Fe-oxides/oxy-hydroxides, leading to the saturation of dissolved Fe in deep pore fluids. Similar to iron, manganese also acts as a good electron acceptor, which could explain the substantial concentrations of Mn (MnO = 0.02-0.6%, Table 2) in siderites. Among other major elements, Na, K, and P contents show minor variations between HMC and siderite concretions at different core depths (Table 2).

The trace element compositions of High-Mg calcite (HMC) and siderite concretions, which developed under the geochemical regimes of methane oxidation and methanogenesis, respectively, are presented in Table 3. Results show that, despite distinct mineralogy and carbon isotopic ratios, several trace elements, particularly redox-sensitive elements (e.g., V, Cr, Co, Ni, Zn, U) and refractory elements (e.g., Sc, Cs, Ga, Zr, Hf, Nb, Ta, Th), have comparable concentrations in both HMC and siderite deposits. This indicates the limited influence of diagenetic changes on the accretion of these elements.

In marine sediment, the redox condition of pore water plays a crucial role in the mobility of several redox-sensitive trace elements, thus potentially controlling their accretion in associated mineral phases (Ge et al., 2010 and references therein). In other words, the concentrations of these elements in sedimentary carbonates can serve as indicators for the redox condition of the pore fluid in the host sediment. In this study, the concentrations of some of these redox elements, such as V (56-75 ppm), Cr (15-26 ppm), Co (4.5-12 ppm), Zn (20-31 ppm), and U (1-6 ppm) (Table 3), in these carbonate concretions of diagenetic origins are substantially higher than those recorded in typical deep-sea carbonates (V = 20 ppm; Co = 7.0 ppm; Cr = 11 ppm; U < 1.0 ppm; Turekian and Wedepohl, 1961)



or marine limestone, JLs-1 (V = 3 ppm; Co = 0.045 ppm; Zn = 2 ppm; Wang et al., 2019), developed under the direct influence of oxygenated seawater.

In a cold seep environment, reducing conditions promote the release of a substantial amount of trace metals from reducible sedimentary organics and metal oxides into pore fluid, acting as a source for metals in authigenic carbonates (Smrzka et al., 2020 and references therein). Earlier studies have also described the enrichment of redox elements in cold seep carbonates as a result of precipitation under suboxic to anoxic conditions in the sediment (Wang et al., 2019; Ge et al., 2010; Sarkar et al., 2003). In the present study, the concentrations of most of these redox elements (except U) show negligible variation between HMC and siderite, indicating no mineralogical control on their enrichment. Unlike other redox elements, the concentration of U was considerably higher in HMC (average 3.84 ppm) than in siderite (average 1.42 ppm), which could be explained by the preferential incorporation of U within the calcite lattice. A previous experimental study by Sturchio et al. (1998) indicates that effective sequestration of  $U^{4+}$  species by calcite developed under reducing conditions can cause an elevated concentration of U.

The High-Mg calcite (HMC) and siderite concretions from the NGHP-01-10D core also exhibited significant enrichment in particle-reactive, high field strength elements (HFSE) such as Zr (43-92 ppm), Nb (4-7 ppm), Hf (1-2.5 ppm), and Ta (0.2-0.7 ppm) (Table 3), in comparison to common marine carbonates (Zr ~20 ppm, Nb ~4.6 ppm, Hf ~0.41 ppm, Ta <0.1 ppm; Turekian and Wedepohl, 1961). This suggests that the concentrations of dissolved HFSE in sedimentary pore fluids for authigenic cold-seep carbonates were significantly higher than those in natural deep seawater (Frimmel, 2009). The characteristic weight ratios of these geochemical twins in both HMC and siderite, such as Zr/Hf (29.6-72.9, average 38.9) and Nb/Ta (6.6-26, average 14.9) (Table 3), were lower than typical deep seawater values (Zr/Hf =150-300; Nb/Ta =15-22; Firdaus et al., 2011). However, these estimated ratios in authigenic carbonates were close to the average values in the upper continental crust (e.g., Zr/Hf =36.3-38.7, David et al., 2000; Nb/Ta =12-13, Barth et al., 2000), indicating a possible contribution of crustal materials in the genesis of these cold-seep carbonates (Fig. 7).

Numerous earlier studies have indicated that various terrestrial components, such as erosional products from rocks, sediment, and organics, reached this marginal basin through fluvial fluxes of major rivers and rapidly became buried due to the fast rate of sedimentation (Phillips et al., 2014; Johnson et al., 2014; Kocherla et al., 2015). Therefore, the elements adsorbed on detrital matter, as well as those present within the siliciclastic minerals of terrestrial origin, might be responsible for the excess HFSE in these cold-seep carbonates (Firdaus et al., 2011). Similar to HFSE, the elevated

concentrations of other refractory elements such as Sc (7.3-9.5 ppm), Cs (0.5-1.0 ppm), Ga (7.8-12.6 ppm), and Th (3.3-5.3 ppm) (Table 3) in these authigenic carbonates suggest that, besides seawater sources, these water-insoluble elements might also be contributed by diagenetic changes in detrital materials deposited in that marginal basin. Furthermore, there was no distinct variation in these refractory elements between HMC and siderite (Table 3), suggesting that mineralogy and mineral-specific evolutionary processes may not have a major impact on their concentration.

Strontium (Sr) concentrations exhibited widely variable values in both types of cold-seep carbonates (227-1132 ppm, Table 3) developed in anoxic environments. However, these values were lower than those typically found in deep-sea carbonates (Sr ~2000 ppm; Turekian and Wedepohl, 1961) originating from seawater. This suggests that diagenetic processes involved in the genesis of seep carbonates and/or mineralogy might control the incorporation of Sr into these authigenic carbonates. It is also noteworthy that the Sr contents in High-Mg calcite (HMC) (954-1132 ppm, average ~1027 ppm) within the shallow sediments were significantly higher than the values found in siderites (227-669 ppm, average ~337 ppm) at deeper depths (Table 3). The minor concentration of strontianite ( $\text{SrCO}_3$ ) in HMC concretions (Table 1) also suggests a favorable environmental condition for Sr precipitation within the shallow methane oxidation zone.

Close to the Sulfate-Methane Transition Zone (SMTZ), the production of dissolved inorganic carbon via the oxidative consumption of methane, coupled with a significant influx of dissolved strontium (Sr) from infiltrating seawater, likely promotes the formation of strontium in conjunction with calcium carbonate precipitation. Moreover, studies have shown that dissolved  $\text{Sr}^{2+}$  ions could be incorporated into the calcite structure developing from saturated  $\text{CaCO}_3$  solutions (Matsunuma et al., 2014). A similar incorporation mechanism of  $\text{Sr}^{2+}$  within the calcite or aragonite lattice could also be responsible for Sr enrichment in HMC concretions. Conversely, in sedimentary layers primarily composed of siderite, the occurrence of strontianite ( $\text{SrCO}_3$ ) mineralization was infrequently observed (refer to Table 2).

This observation suggests that there may be an insufficient concentration of  $\text{Sr}^{2+}$  in the pore water of the deeper sediment, potentially limiting significant  $\text{SrCO}_3$  precipitation. In contrast to Sr, other alkali metals (e.g., Rb) or alkaline earth metals (e.g., Ba) exhibited relatively low but comparable concentrations in both High-Mg calcite (HMC) (Ba= 110-135 ppm; Rb= 19.6-24 ppm) and siderite (Ba= 114-202 ppm; Rb= 13.7-18 ppm) (refer to Table 3). This result implies that the low concentrations of Ba and Rb in both HMC and siderite may be attributed to the absence of preferential lattice-bound cationic substitution with larger  $\text{Ba}^{2+}$  or  $\text{Rb}^{2+}$  ions in either type of authigenic carbonates. However, the comparable concentration of Ba in both HMC and siderite,

along with the trace appearance of witherite ( $\text{BaCO}_3$ ) at all depths (Table 2), suggests substantial Ba concentrations in pore fluids at these sedimentary depths.

#### ***4.3. REE systematics of calcite and siderite: A comparative assessment between the factors responsible for their genesis-***

The REE systematics of authigenic carbonates in cold seep environments can provide crucial constraints on various diagenetic processes involved in their genesis and reflect the fluid characteristics from which they precipitated (Ge et al., 2010; Novikova et al., 2015; Franchi et al., 2017; Smrzka et al., 2019; Zhang et al., 2023). Previous studies have shown that features such as bulk REE contents and shale-normalized REE patterns may considerably vary in seep carbonates with different mineralogy and/or developed under different environmental conditions (Rongemaille et al., 2011; Wang et al., 2014).

The analyses of the carbonate concretions from the K-G basin showed that the total rare earth contents ( $\Sigma\text{REE}$ ) vary within the range of 41 to 103 ppm (Table 4). These REE contents in K-G basin carbonates are mostly comparable to the higher-end values of several other authigenic carbonates studied elsewhere ( $\Sigma\text{REE}=0.1$  to  $\sim 85$  ppm; Feng et al., 2009b; Ge et al., 2010; Novikova et al., 2015; Yang et al., 2022; Zhang et al., 2023); and also more than those reported in marine limestone ( $\Sigma\text{REE}=28$  ppm, Bellanca et al., 1997). Such enhanced REE concentrations in authigenic carbonates suggest that there was a substantial availability of dissolved REE in source fluids and stable carbonate compounds in seep carbonates.

In particular, diagenetic alterations of detrital materials could be a prominent source for REEs in such authigenic carbonates. Furthermore, the HMC concretions show a depleted range of  $\Sigma\text{REE}$  (41-80 ppm) compared to those in siderite (42-102 ppm) from deeper sediment (Table 4). Previous studies on authigenic carbonate deposits also indicated that REE accretion in carbonates may differ with mineralogy, and the REE contents in siderite deposits are usually higher than Fe-depleted carbonates (Rongemaille et al., 2011; Wang et al., 2014; Smrzka et al., 2020).

The Post Archaean Australian Shale (PAAS) normalized REE-Y patterns of HMC from shallow sediment depths are relatively flat and closely resemble each other (Fig. 8A). In these patterns, the degree of fractionation between light and heavy REEs, as estimated by the shale-normalized  $\text{Nd}_n/\text{Ybn}$  ratio ( $=0.95$ - $0.98$ , Table 4), indicates a lack of any cross-group fractionations. These flat normalized REE patterns are comparable to the patterns reported in many other calcite-dominated cold seep carbonates described elsewhere (Feng et al., 2009b; Ge et al., 2010; Yang et al., 2022). However, those flat REE patterns of HMC considerably differ from those of siderites, which were

characterized by progressive HREE enrichment ( $Ndn/Ybn = 0.3 - 0.6$ ; Table 4; Fig. 7B). Such marginal REE cross-group fractionations in siderite might be indicative of elevated concentrations of HREEs in source fluids, originating in the deeper horizons of methanogenesis. In a previous study, similar enrichment of HREE in pore fluids of deep methanogenic regimes of marine sedimentary columns was also evidenced by Kim et al. (2012). The same investigation further indicated that processes involved in the degradation of particulate organics during active methanogenesis are primarily responsible for the preferential regeneration of organic-bound dissolved HREE in pore water. In the K-G basin, the high sedimentation rate enhances the supply of particulate organics and the rate of methanogenic reactions (Solomon et al., 2014), which is apparently responsible for the relative enrichment of HREE in both pore fluid and seep carbonate.

The REE-Y patterns of both authigenic HMC and siderite concretions did not show any perceptible Ce-anomalies ( $Ce/Ce^* = 0.89 - 0.96$ ), but traces of positive Eu anomalies ( $Eu/Eu^* = 1.15 - 1.36$ ; Fig. 7; Table 4). The lack of Ce-anomalies in these carbonates distinctly differs from intense negative Ce-anomalies ( $Ce/Ce^* < 0.9$ ) usually found in marine limestone developed in oxic or sub-oxic marine environments (Özyurt et al., 2020 and references therein); but is very similar to those found in many other cold-seep carbonates at the China Sea (Ge et al., 2010; Wang et al., 2014; Yang et al., 2022); and the Gulf of Mexico (Feng et al., 2013). This result confirms the anoxic formation conditions for the genesis of both carbonates at different sediment depths in the K-G basin. The origins of minor positive Eu anomalies in HMC and siderite deposits are not very clear. Still, the presence of detrital minerals like Na-feldspar characteristic with positive Eu anomalies (Murray et al., 1991) could be a possible source for such minor Eu anomalies.

Owing to similar charge and ionic radii, the geochemical properties of yttrium are similar to those of holmium, and therefore, Y is often referred to as a pseudo-lanthanide. For such coherent geochemical behaviors, Y and Ho act as a twin pair in various natural systems, and their ratios possess very consistent values in many geological components. In the present study, except for the high Y/Ho ratio ( $=142$ ) in siderite from 179 mbsf, the rest of the values lie within the range between 24 and 45 (Table 4); which are very comparable to other cold seep carbonates from the Black Sea ( $Y/Ho = 24-39$ ; Novikova et al., 2015). However, the average Y/Ho ratios ( $=28.4$ ) in both HMC and siderite are lower than the values in pure marine limestone ( $Y/Ho \sim >36 - 60$ ; Özyurt et al., 2020); but close to those reported in the upper continental crusts (av.  $Y/Ho = 26.2 \pm 0.36$ ; Kamber et al., 2005). This result indicates the contribution of elements from terrestrial matter and a limited supply of these elements from seawater ( $Y/Ho \sim 60$ ) into the source fluids of these cold seep carbonates.

## 5. Conclusions

In the KG Basin, gas-hydrate-associated authigenic carbonates within a sediment core exhibit a prevalence of Mg-rich calcites in shallower regions and siderites in deeper segments of the core. The lighter carbon-isotope compositions of calcite in shallow sediment affirm its genesis involving anaerobic methane oxidation, while isotopically heavier siderites at deeper levels may develop through microbial methanogenesis. Despite the distinct formation mechanisms of these two types of authigenic carbonates, their oxygen-isotope ratios and the majority of their elemental compositions fall within a close range of values, suggesting that their concentrations were independent of diagenetic changes in the sediment.

Furthermore, certain comparable elemental indices in both carbonate types confirm that the features of source fluids, such as reduced conditions and compositions analogous to the crust, are consistent throughout the sedimentary column. However, in contrast, the bulk compositions of a few trace and major elements distinctly differ in these cold-seep carbonates, primarily due to the geochemical variability of their source fluids and cationic substitution in mineral phases. The compositional diversity of the source fluid arises from diverse contributions from detrital matter and varying degrees of reductive dissolution of metallic oxides in the sediment.

**Acknowledgments** We thank the Directors, CSIR-NIO, Goa, and CSIR-NGRI, Hyderabad for providing the necessary facilities for this study. This research work was funded by the National Gas Hydrate Program of India. The DGH is thanked for providing samples for the present study. Thanks to Drs. A. Mazumdar, P. Dewangan, and M. Judith, for their valuable inputs on this present investigation. The authors also thank Mr. G. Prabhu and Mr. V. Khedekar for the XRD and SEM analyses respectively. This is NIO contribution no. XXXX.

### **Credit author statement**

*Muralidhar Kocherla and Durbar Ray:* Conceptualization, Methodology, Draft preparation.  
*Manavalan Satyanarayanan, Maria Hilda João and Christo Sojan:* Methodology, Resources, Data curation, Formal analysis, draft preparation.

### **Declaration of competing interest**

The authors declare that they have no known competing financial interests or personal relationships that could have appeared to influence the work reported in this paper.

## References

- Aloisi, G., Pierre, C., Rouchy, J., Foucher, J., Woodside, J., MEDINAUT Scientific Party, 2000. Methane-related authigenic carbonates of eastern Mediterranean Sea mud volcanoes and their possible relation to gas hydrate destabilization. *Earth Planet. Sci. Lett.* 184, 321-338. [https://doi.org/10.1016/S0012-821X\(00\)00322-8](https://doi.org/10.1016/S0012-821X(00)00322-8).
- Balaram, V., Gnaneshwar Rao, T., 2003. Rapid determination of REEs and other trace elements in geological samples by microwave acid digestion and ICP-MS. *Atom. Spec.*, 24, 206–212.
- Barth, M.G., McDonough, W.F., Rudnick, R.L., 2000. Tracking the budget of Nb and Ta in the continental crust. *Chem. Geol.*, 165, 197-213. [https://doi.org/10.1016/S0009-2541\(99\)00173-4](https://doi.org/10.1016/S0009-2541(99)00173-4).
- Bayon, G., Pierre, C., Etoubleau, J., Voisset, M., Cauquil, E., Marsset, T., Sultan, N., Le Drezen, E., Fouquet, Y., 2007. Sr/Ca and Mg/Ca ratios in Niger Delta sediment: Implications for authigenic carbonate genesis in cold seep environments. *Mar. Geol.*, 241, 93-109. <https://doi.org/10.1016/j.margeo.2007.03.007>.
- Bellanca, A., Muetti, D., Neri, R., 1997. Rare earth elements in limestone/mudstone couplets from the Albian–Cenomanian Cismon section (Venetian region, north Italy): assessing REE sensitivity to environmental changes. *Chem. Geol.*, 141, 141–152. [https://doi.org/10.1016/S0009-2541\(97\)00058-2](https://doi.org/10.1016/S0009-2541(97)00058-2).
- Boetius, A., Ravensschlag, K., Schubert, C.J., Rickert, D., Widdel, F., Giesecke, A., Amann, R., Jørgensen, B.B., Witte, U., Pfannkuche, O., 2000. A marine microbial consortium apparently mediates anaerobic oxidation of methane. *Nature*, 407, 623-626.
- Bojanowski, M.J., Baginski, B., Guillermier, C., Franchi, I.A., 2015. Carbon and oxygen isotope analysis of hydrate-associated Oligocene authigenic carbonates using NanoSIMS and IRMS. *Chem. Geol.*, 416, 51-64. <https://doi.org/10.1016/j.chemgeo.2015.10.021>.
- Collett, T.S., Riedel, M., Cochran, J.R., Boswell, R., Kumar, P., Sathe, A.V. 2008. Indian continental margin gas hydrate prospects: Results of The Indian National Gas Hydrate Program (NGHP) Expedition 01. Proceedings of the 6th International Conference on Gas Hydrates (ICGH 2008), Vancouver, British Columbia, Canada, July 6-10, 2008. <https://doi.org/10.7916/d8-nf9w-cz91>.
- David, K., Schiano, P., Allegre, C.J., 2000. Assessment of the Zr/Hf fractionation in oceanic basalts and continental materials during petrogenetic processes. *Earth Planet. Sci. Lett.*, 178, 285-301. [https://doi.org/10.1016/S0012-821X\(00\)00088-1](https://doi.org/10.1016/S0012-821X(00)00088-1).
- Degens, E.T., Epstein, S., 1964. Oxygen and carbon isotope ratios in coexisting calcites and dolomites from recent and ancient sediments. *Geochim. Cosmochim. Acta*, 28, 23-44. [https://doi.org/10.1016/0016-7037\(64\)90053-5](https://doi.org/10.1016/0016-7037(64)90053-5).
- Dewangan, P., Ramprasad, T., Ramana, M.V., Mazumdar, A., Desa, M., Badesab, F.K., 2010. Seabed morphology and gas venting features in the continental slope region of Krishna-Godavari basin, Bay of Bengal: Implications in Gas-Hydrate Exploration. *Mar. Pet. Geol.*, 27, 1628-1641. <https://doi.org/10.1016/j.marpetgeo.2010.03.015>.
- Elderfield, H., Sholkovitz, E.R., 1987. Rare earth elements in the pore waters of reducing nearshore sediments. In *Earth and Planetary Science Letters* (Vol. 82). Elsevier Science Publishers B.V. [https://doi.org/10.1016/0012-821X\(87\)90202-0](https://doi.org/10.1016/0012-821X(87)90202-0).

- Feng, D., Chen, D.F., Roberts, H.H., 2009a. Petrographic and geochemical characterization of seep carbonate from Bush Hill (GC 185) gas vent and hydrate site of the Gulf of Mexico. *Mar. Petrol. Geol.*, 26, 1190-1198. <https://doi.org/10.1016/j.marpetgeo.2008.07.001>.
- Feng, D., Chen, D.F., Peckmann, J., 2009b. Rare earth elements in seep carbonates as tracers of variable redox conditions at ancient hydrocarbon seeps. *Terra Nova*, 21(1), 49-56. <https://doi.org/10.1111/j.1365-3121.2008.00855.x>.
- Feng, D., Lin, Z., Bian, Y., Chen, D., Peckmann, J., Bohrmann, G., Roberts, Harry H. 2013. Rare earth elements of modern seeps from the Gulf of Mexico, the Black Sea, and the Congo Fan. *PANGAEA*, <https://doi.org/10.1594/PANGAEA.834248>.
- Firdaus, M.L., Minami, T., Norisuye, K., Sohrin Y. 2011. Strong elemental fractionation of Zr–Hf and Nb–Ta across the Pacific Ocean. *Nat. Geosci.* 4, 227–230.
- Franchi, F., Rovere, M., Gamberi, F., Rashed, H. Vaselli, O., Tassi F. 2017. Authigenic minerals from the Paola Ridge (southern Tyrrhenian Sea): Evidences of episodic methane seepage *Mar. Petrol. Geol.*, 86, 228-247. <https://doi.org/10.1016/j.marpetgeo.2017.05.031>.
- Frimmel, H.E., 2009. Trace element distribution in Neoproterozoic carbonates as palaeo-environmental indicator. *Chem. Geol.* 258, 338-353. <https://doi.org/10.1016/j.chemgeo.2008.10.033>.
- Gaikwad, V., Badesab, F., Dewangan, P., Kotha, M., 2021. Diagenesis of magnetic minerals in active and relict methane seep: Constraints from rock magnetism and mineralogical records from Bay of Bengal. *Front. Earth Sci.* 9, 638594. doi: 10.3389/feart.2021.638594. <https://doi.org/10.3389/feart.2021.638594>.
- Ge, L., Jiang, S.Y., Swennen, R., Yang, T., Yang, J.H., Yu, N.Y., Liu, J., Chen, D.H., 2010. Chemical environment of cold seep carbonate formation on the northern continental slope of South China sea: Evidence from trace and rare earth geochemistry. *Mar. Geol.*, 277, 21-30. <https://doi.org/10.1016/j.margeo.2010.08.008>.
- Gieskes, J., Mahn, C., Day, S., Martin, J.B., Greinert, J., Rathburn, T., MacAdoo, B., 2005. A study of the chemistry of pore fluids and authigenic carbonates in methane seep environments: Kodiak Trench, Hydrate Ridge, Monterey Bay, and Eel River Basin. *Chem. Geol.* 220, 329–345. <https://doi.org/10.1016/j.chemgeo.2005.04.002>.
- Greinert, J., Bohrmann, G., Suess, E., 2001. Gas hydrate-associated carbonates and methane-venting at Hydrate Ridge: Classification and distribution and origin of authigenic lithologies. In: Paull, C.K., and Dillon, P.W. (eds), *Natural Gas Hydrates: Occurrence, Distribution, and Dynamics*. *Geophys. Monogr.*, Washington DC: American Geophysical Union 124, 99-113.
- Haley, B.A., Klinkhammer, G.P. 2003. Complete separation of rare earth elements from small volume samples by automated ion chromatography: method development and application to benthic flux. *Mar Chem* 82, 197–220. [https://doi.org/10.1016/S0304-4203\(03\)00070-7](https://doi.org/10.1016/S0304-4203(03)00070-7).
- Han, M.W., Suess, E., 1989. Subduction-induced pore fluid venting and the formation of authigenic carbonates along the Cascadia continental margin: Implications for the global Ca-cycle. *Palaeogeogr. Palaeoclimatol. Palaeoecol.*, 71, 97-118. [https://doi.org/10.1016/0031-0182\(89\)90032-1](https://doi.org/10.1016/0031-0182(89)90032-1).

- Harvey, P.K., Atkin, B.P. 1981. The Rapid determination of Rb, Sr and their ratios in geological materials by X-Ray Fluorescence Spectrometry using a Rhodium X-Ray tube. In *Chemical Geology* (Vol. 32). [https://doi.org/10.1016/0009-2541\(81\)90150-9](https://doi.org/10.1016/0009-2541(81)90150-9).
- Hesse, R. 2003. Pore Water Anomalies of Submarine Gas-Hydrate Zones as Tool to Assess Hydrate Abundance and Distribution in the Subsurface: What Have We Learned in the Past Decade? *Earth-Sci. Rev.* 61, 149–179. [https://doi.org/10.1016/S0012-8252\(02\)00117-4](https://doi.org/10.1016/S0012-8252(02)00117-4).
- Hinrichs, K.U., Hayes, J.M., Sylva, S.P., Brewer, P.G., Delong, E.F., 1999. Methane-consuming archaeobacteria in marine sediments, *Nature*, 398, 802-805.
- Himmler, T., Bach, W., Bohrmann, G., Peckmann, J. 2010. Rare earth elements in authigenic methane-seep carbonates as tracers for fluid composition during early diagenesis. *Chem. Geol.* 277, 126-136. <https://doi.org/10.1016/j.chemgeo.2010.07.015>.
- Hovland, M., Talbot, M.R., Qvale, H., Olausen, S., Aasberg, L. 1987. Recently formed methane-derived carbonates from the North Sea. *J. Sed. Petrol.* 57, 881-892.
- Hu, Y., Feng, D., Peckmann, J., Roberts, H. H., Chen, D. 2014. New insights into cerium anomalies and mechanisms of trace metal enrichment in authigenic carbonate from hydrocarbon seeps. *Chem. Geol.*, 381, 55–66. <https://doi.org/10.1016/j.chemgeo.2014.05.014>
- Johnson, J.E., Phillips, S.C., Torres, M.E., Pinerro, E., Rose, K., Giosan, L. 2014. Influence of total organic carbon deposition on the inventory of gas hydrate in the Indian continental margins. *Mar. Pet. Geol.* 58, 406e424. <https://doi.org/10.1016/j.marpetgeo.2014.08.021>.
- Jones, B., Manning, D.A.C. 1994. Comparison of geochemical indices used for the interpretation of palaeoredox conditions in ancient mudstones. *Chem. Geol.*, 111, 111–129. [https://doi.org/10.1016/0009-2541\(94\)90085-X](https://doi.org/10.1016/0009-2541(94)90085-X).
- Kamber, B.S., Greig, A., Collerson, K.D. 2005. A new estimate for the composition of weathered young upper continental crust from alluvial sediments, Queensland, Australia. *Geochim. Cosmochim. Acta*, 69(4), 1041-1058. <https://doi.org/10.1016/j.gca.2004.08.020>.
- Kim, J.H., Torres, M.E., Haley, B.A., Kastner, M., Pohlman, J.W., Riedel, M., Lee, Y.J. 2012. The effect of diagenesis and fluid migration on rare earth element distribution in pore fluids of the northern Cascadia accretionary margin. *Chem. Geol.*, 291, 152–165. <https://doi.org/10.1016/j.chemgeo.2011.10.010>.
- Kocherla, M., Mazumdar, A., Karisiddaiah, S.M., Borole D.V., Rao., B.R. 2006. Evidences of methane derived authigenic carbonates from the sediments of the Krishna–Godavari Basin, eastern continental margin of India. *Curr. Sci.*, 91, 318-323. <https://www.jstor.org/stable/24094137>.
- Kocherla, M., Teichert, B.M., Pillai, S., Satyanarayanan, M., Ramamurty, P.B., Patil, D.J., Rao, A.N. 2015. Formation of methane-related authigenic carbonates in a highly dynamic biogeochemical system in the Krishna–Godavari Basin, Bay of Bengal. *Mar. Petrol. Geol.* 64, 324–333. <https://doi.org/10.1016/j.marpetgeo.2015.02.034>.
- Lee, M., Collett, T. 2009. Gas hydrate saturations estimated from fractured reservoir at Site NGHP-01-10, Krishna-Godavari Basin, India. *J. Geophys. Res.* 114(B7), B07102. <https://doi.org/10.1029/2008JB006237>.



- Lumsden, D.S., 1979. Discrepancy between thin-section and x-ray estimates of dolomite in limestone. *J. Sed. Petrol.* 49, 429–436. <https://doi.org/10.1306/212F7761-2B24-11D7-8648000102C1865D>.
- Matsunuma, S., Kagi, H., Komatsu, K., Maruyama, K., Yoshino, T. 2014 Doping incompatible elements into calcite through amorphous calcium carbonate. *Cryst. Growth Des.*, 14(11), 5344-5348.
- Mazumdar, A., Dewangan, P., João, H.M., Peketi, A., Khosla, V.R., Kocherla, M., Badesab, F.K., Joshi, R.K., Roxanne, P., Ramamurty, P.B., Karisiddaiah., S.M., Patil, D.J., Dayal, A.M., Ramprasad, T., Hawkesworth, C.J., Avanzinelli, R. 2009. Evidence of paleo–cold seep activity from the Bay of Bengal, offshore India. *Geochem. Geophys. Geosys.*, 10(6), 1-15. <https://doi.org/10.1029/2008GC002337>.
- Mazzini, A., Svensen, H., Hovland, M., Planke, S. 2006. Comparison and implications from strikingly different authigenic carbonates in a Nyegga complex pockmark, G11, Norwegian Seas. *Mar. Geol.*, 231, 89-102. <https://doi.org/10.1016/j.margeo.2006.05.012>.
- Mozley, P.S., Carothers, W.W. 1992. Elemental and isotopic composition of Fe-rich carbonate in the Kuparuk formation, Alaska: effect of microbial activity and water/sediment interaction on early pore-water chemistry. *J. Sediment. Petrol.*, 62, 681-692. <https://doi.org/10.1306/D4267988-2B26-11D7-8648000102C1865D>.
- Murray, R.W., Brink, M.R.B. Gerlach, D.C., G.P. Russ III, Jones, D.L. 1991. Rare earth, major and trace elements in chert from the Franciscan complex and Monterey group. California: Assessing REE sources to fine-grained marine sediments, *Geochim. Cosmochim. Acta.* 55, 1875-1895. [https://doi.org/10.1016/0016-7037\(91\)90030-9](https://doi.org/10.1016/0016-7037(91)90030-9).
- Naehr, T.H., Eichhubl, P., Orphan, V.J., Hovland, M., Paull, C.K., Ussler, III.W., Lorenson, T.D., Greene, H.G. 2007. Authigenic carbonate formation at hydrocarbon seeps in continental margin sediments: a comparative study. *Deep Sea Res. (Part II)*, 54,1268-1291. <https://doi.org/10.1016/j.dsr2.2007.04.010>.
- Novikova, S.A., Shnyukov, Y.A., Sokol, E.V., Kozmenkov, O.A., Semenova, D.V., Kutny, V.A. 2015. A methane-derived carbonate build-up at a cold seep on the Crimean slope, north-western Black Sea. *Mar. Geol.*, 363, 160-173. <https://doi.org/10.1016/j.margeo.2015.02.008>.
- Ojha, P.S., Dubey, M. 2006. Gaint hydrocarbon fields of offshore Krishna-Godavari Basin. Petroview 1, published by Directorate General of Hydrocarbons, New Delhi, 26-30.
- Özyurt, M., Kırmac, M.Z., Al-Aasm, I., Hollis, C., Tasl, K., Kandemir, R. 2020. REE characteristics of lower cretaceous limestone succession in Gümüşhane, NE Turkey: Implications for ocean palaeoredox conditions and diagenetic alteration. *Mineral*, 10, 683, doi:10.3390/min10080683.
- Peckmann, J., Birgel, D., Kiel, S. 2009. Molecular fossils reveal fluid composition and flow intensity at a Cretaceous seep. *Geol.*, 37, 847-850. <https://doi.org/10.1130/G25658A.1>.
- Peckmann, J., Thiel, V. 2004. Carbon cycling at ancient methane-seep. *Chem. Geol.* 205, 443-467. <https://doi.org/10.1016/j.chemgeo.2003.12.025>.

- Phillips, S.C., Johnson, J.E., Underwood, M.B., Guo, J., Giosan, L., Rose, K., 2014. Long time scale variation in bulk and clay mineral composition of Indian continental margin sediments in the Bay of Bengal, Arabian Sea, and Andaman Sea. *Mar. Pet. Geol.* 58, 117e138. <https://doi.org/10.1016/j.marpetgeo.2014.06.018>.
- Prabhakar, K.N., Zutshi, P.L. 1993. Evolution of southern part of Indian east coast basins. *J. Geol. Soc. Ind.* 41, 215-230.
- Ramana, M.V., Nair, R.R., Sarma, K.V.L.N.S., Ramprasad, T., Krishnaa, K.S., Subrahmanyam, V., D'Cruza, M., Subrahmanyam, C., Paul, J., Subrahmanyam, V.D., Chandra Sekhar, V., 1994. Mesozoic anomalies in the Bay of Bengal. *Earth Planet. Sci. Lett.* 121, 469–475. [https://doi.org/10.1016/0012-821X\(94\)90084-1](https://doi.org/10.1016/0012-821X(94)90084-1).
- Ramana, M.V, Ramprasad, T, KameshRaju., K.A., Desa., M. 2007. Occurrence of gas hydrates along the continental margins of India, particularly the Krishna-Godavari offshore basin. *Int. J. Environ. Stud.*, 64, 675-693. <https://doi.org/10.1080/00207230701476321>.
- Ramprasad, T., Dewangan, P., Ramana, M.V., Mazumdar, A., Karisiddaiah, S.M., Ramya, E.R., Sriram, G. 2011. Evidence of slumping/sliding in Krishna-Godavari offshore basin due to gas/fluid movements. *Mar. Petrol. Geol.*, 28, 1806-1816. <https://doi.org/10.1016/j.marpetgeo.2011.02.007>.
- Rao, G.N. 2001. Sedimentation, stratigraphy, and petroleum potential of Krishna-Godavari Basin, East Coast of India. *AAPG Bull.*, 85, 1623-1643. <https://doi.org/10.1306/8626CCDF-173B-11D7-8645000102C1865D>.
- Roberts, H.H., Feng, D., Joye, S.B. 2010. Cold-seep carbonates of the middle and lower continental slope, northern Gulf of Mexico. *Deep-Sea Res. II*, 57, 2040-2054. <https://doi.org/10.1016/j.dsr2.2010.09.003>.
- Roberts, H.H., Aharon, P., Walsh, M.M. 1993. Cold-seep carbonates of the Louisiana continental slope-to-basin floor. In: Rezal, R., and Lavoie, D.L. (Eds), *Carbonate Micro fabrics*, New York, Springer-Verlag, pp. 95-104.
- Rodriguez, N.M., Paull, C.K., Borowski, W.S. 2000. Zonation of authigenic carbonates within gas hydrate-bearing sedimentary sections on the Blake ridge: Offshore southeastern North America. In: *Proceedings of the Ocean Drilling Program, Scientific Results*, (Eds) Paull, C.K., Matsumoto, R., Wallace, P.J., and Dillon, W.P., vol. 164, pp. 301-312.
- Rongemaille, E., Bayon, G., Pierre, C., Bollinger, C., Chu, N.C., Fouquet, Y., Riboulot, V., Voisset, M. 2011. Rare earth elements in cold seep carbonates from the Niger delta. *Chem. Geol.* 286, 196e206. <https://doi.org/10.1016/j.chemgeo.2011.05.001>.
- Ruban, A., Rudmin, M., Dudarev, O., Mazurov, A. 2020. The Formation of Authigenic Carbonates at a Methane Seep Site in the Northern Part of the Laptev Sea. *Minerals*, 10, 948, doi:10.3390/min10110948.
- Sarkar, A., Sarangi, S., Ebihara, M., Battacharya, S.K., Ray, A.K. 2003. Carbonate geochemistry across the Eocene/Oligocene boundary of Kutch, western India: implication of oceanic O<sub>2</sub>-poor condition and foraminiferal extinction. *Chem. Geol.*, 201, 281-293. [https://doi.org/10.1016/S0009-2541\(03\)00238-9](https://doi.org/10.1016/S0009-2541(03)00238-9).

- Scotese, C.R., Gahagan, L.M., Larson, R.L. 1988. Plate tectonic reconstructions of the Cretaceous and Cenozoic ocean basins. *Tectonophys.*, 155, 27-48. [https://doi.org/10.1016/0040-1951\(88\)90259-4](https://doi.org/10.1016/0040-1951(88)90259-4).
- Schier, K., Himmler, T., Lepland, A., Kraemer, D., Schönenberger, J., Bau, M. 2021. Insights into the REY inventory of seep carbonates from the Northern Norwegian margin using geochemical screening. *Chem. Geol.*, 559, 119857. <https://doi.org/10.1016/j.chemgeo.2020.119857>.
- Smrzka, D., Feng, D., Himmler, T., Zwicker, J., Hu, Y., Monien, P., Tribovillard, N., Chen, D., Peckmann, J. 2020. Trace elements in methane-seep carbonates: Potentials, limitations, and perspectives. In *Earth-Science Reviews* (Vol. 208). Elsevier B.V. <https://doi.org/10.1016/j.earscirev.2020.103263>
- Smrzka, D., Zwicker, J., Misch, D., Walkner, C., Gier, S., Monien, P., Bohrmann, G., Peckmann, J. 2019. Oil seepage and carbonate formation: A case study from the southern Gulf of Mexico. *Sedimentology*, 66(6), 2318–2353. <https://doi.org/10.1111/sed.12593>
- Solomon, E.A., Spivack, A.J., Kastner, M., Torres, M.E., Robertson, G. 2014. Gas hydrate distribution and carbon sequestration through coupled microbial methanogenesis and silicate weathering in the Krishna-Godavari basin, offshore India. *Mar. Pet. Geol.*, 58, 233-253. <https://doi.org/10.1016/j.marpetgeo.2014.08.020>.
- Sturchio, N.C., Antonio, M.R., Soderholm, L., Sutton, S.R., Brannon, J.C. 1998. Tetravalent uranium in calcite. *Science*, 281, 971-973. <https://doi.org/10.1126/science.281.5379.971>.
- Suess, E., Torres, M., Bohrmann, G. 1999. Gas hydrate destabilization: Enhanced dewatering, benthic material turnover and large methane plumes at the Cascadia convergent margin. *Earth Planet. Sci. Lett.*, 170, 1-15. [https://doi.org/10.1016/S0012-821X\(99\)00092-8](https://doi.org/10.1016/S0012-821X(99)00092-8).
- SuryaPrakash, L., Ray, D., Paropkari, A.L., Mudholkar, A.V., Satyanarayanan, M., Sreenivas, B., Chandrasekharam, D., Kota, D., Kamesh Raju, K.A., Kaisary, S., Balaram, V., Gurav, T. 2012. Distribution of REEs and yttrium among major geochemical phases of marine Fe-Mn-oxides: Comparative study between hydrogenous and hydrothermal deposits. *Chem. Geol.*, 312–313, 127–137. <https://doi.org/10.1016/j.chemgeo.2012.03.024>.
- Taylor, S.R. and McLennan, S.M., 1985. *The Continental Crust: Its Composition And Evolution*, Blackwell, Malden, Mass.
- Teichert, B.M.A., Bohrmann, G. 2005. Data report: Composition of authigenic carbonates in sediments of the Cascadia accretionary prism, ODP Leg 204. In Tréhu, A.M., Bohrmann, G., Torres, M.E., and Colwell, F.S. (Eds.), *Proc. ODP, Sci. Results*, 204, pp. 1–8.
- Teichert, B.M.A., Johnson, J.E., Solomon, E.A., Giosan, L., Rose, K., Kocherla, M., Connolly, E.C., Torres, M.E. 2014. Composition and origin of authigenic carbonates in the Krishna-Godavari and Mahanadi Basins, eastern continental margin of India. *Mar. Petrol. Geol.*, 58, 438–460. <https://doi.org/10.1016/j.marpetgeo.2014.08.023>.
- Torres, M.E., Bohrmann, G. 2003. Formation of modern and Paleozoic stratiform barite at cold methane seeps on continental margins. In *Geology* (Vol. 897). <http://pubs.geoscienceworld.org/gsa/geology/article-pdf/31/10/897/3525081/i0091-7613-31-10-897.pdf>.

- Torres, M.E., Bohrmann, G., Suess, E. 1996. Authigenic barites and fluxes of barium associated with fluid seeps in the Peru subduction zone. In *EPSL Earth Planet. Sci. Lett.* 144). [https://doi.org/10.1016/S0012-821X\(96\)00163-X](https://doi.org/10.1016/S0012-821X(96)00163-X).
- Turekian, K.L., Wedepohl, K.H. 1961. Distribution of elements in some major units of the earth's crust. *Geol. Soc. Am. Bull.* 72, 175–192. [https://doi.org/10.1130/0016-7606\(1961\)72\[175:DOTAIS\]2.0.CO;2](https://doi.org/10.1130/0016-7606(1961)72[175:DOTAIS]2.0.CO;2).
- von Rad, U., Roesch, H., Berner, U., Geyh, M., Marchig, V., Schulz, H. 1996. Authigenic carbonates derived from oxidized methane vented from the Makran accretionary prism off Pakistan. *Mar. Geol.*, 136, 55-77. [https://doi.org/10.1016/S0025-3227\(96\)00017-5](https://doi.org/10.1016/S0025-3227(96)00017-5).
- Wang, S., Yan, W., Chen, Z., Zhang, N., Chen, H. 2014. Rare earth elements in cold seep carbonates from the southwestern Dongsha area, northern South China sea. *Mar. Petrol. Geol.*, 57, 482-493. <https://doi.org/10.1016/j.marpetgeo.2014.06.017>.
- Wang, X., Bayon, G., Kim, J.H., Lee, D.H., Kim, D., Gueguen, B., Rouget, M.L., Barrat, J.A., Toffin, L., Feng, D. 2019. Trace element systematics in cold seep carbonate and associated lipid compounds. *Chem. Geol.*, 528, 119277. <https://doi.org/10.1016/j.chemgeo.2019.119277>.
- Wignall, P.B., Twitchett, R.J. 1996. Oceanic anoxia and the end Permian mass extinction. *Science*, 272, 1155–1158. <https://doi.org/10.1126/science.272.5265.1155>.
- Yang, K., Zhu, Z., Dong, Y., Zhang, W., Chu, F. 2022. Petrology and geochemistry of cold seep carbonates from the northern Okinawa Trough, East China Sea: implications to early diagenesis. *J. Oceanol. Limnol.*, 40 (4), 1388-1403.
- Yang, S., Liu, L., Chen, H., Tang, G., Luo, L., Liu, N., Cheng, T., Li, D. 2021. Variability and environmental significance of organic carbon isotopes in Ganzi loess since the last interglacial on the eastern Tibetan Plateau. *Catena*, 196, 104866. <https://doi.org/10.1016/j.catena.2020.104866>.
- Zhang, W., Chen, C., Su, P., Wan, Z., Huang, W., Shang, J., Liang, J., Feng, J., Zhou, W., Zhong, L. 2023. Formation and implications of cold seep carbonates in southern South China Sea. *J. Asian Earth Sci.* 241, 105485. <https://doi.org/10.1016/j.jseaes.2022.105485>
- Zhao, M.Y., Zheng, Y.F. 2014. Marine carbonate records of terrigenous input into Paleotethyan seawater: Geochemical constraints from Carboniferous limestones. *Geochim. Cosmochim. Acta*, 141, 508-531, <https://doi.org/10.1016/j.gca.2014.07.001>.
- Zwicker, J., Smrzka, D., Gier, S., Goedert, J.L., Peckmann, J. 2015. Mineralized conduits are part of the uppermost plumbing system of Oligocene methane-seep deposits, Washington State (USA). *Mar. Petrol. Geol.*, 66, 616–630. <https://doi.org/10.1016/j.marpetgeo.2015.05.035>.

Figures:

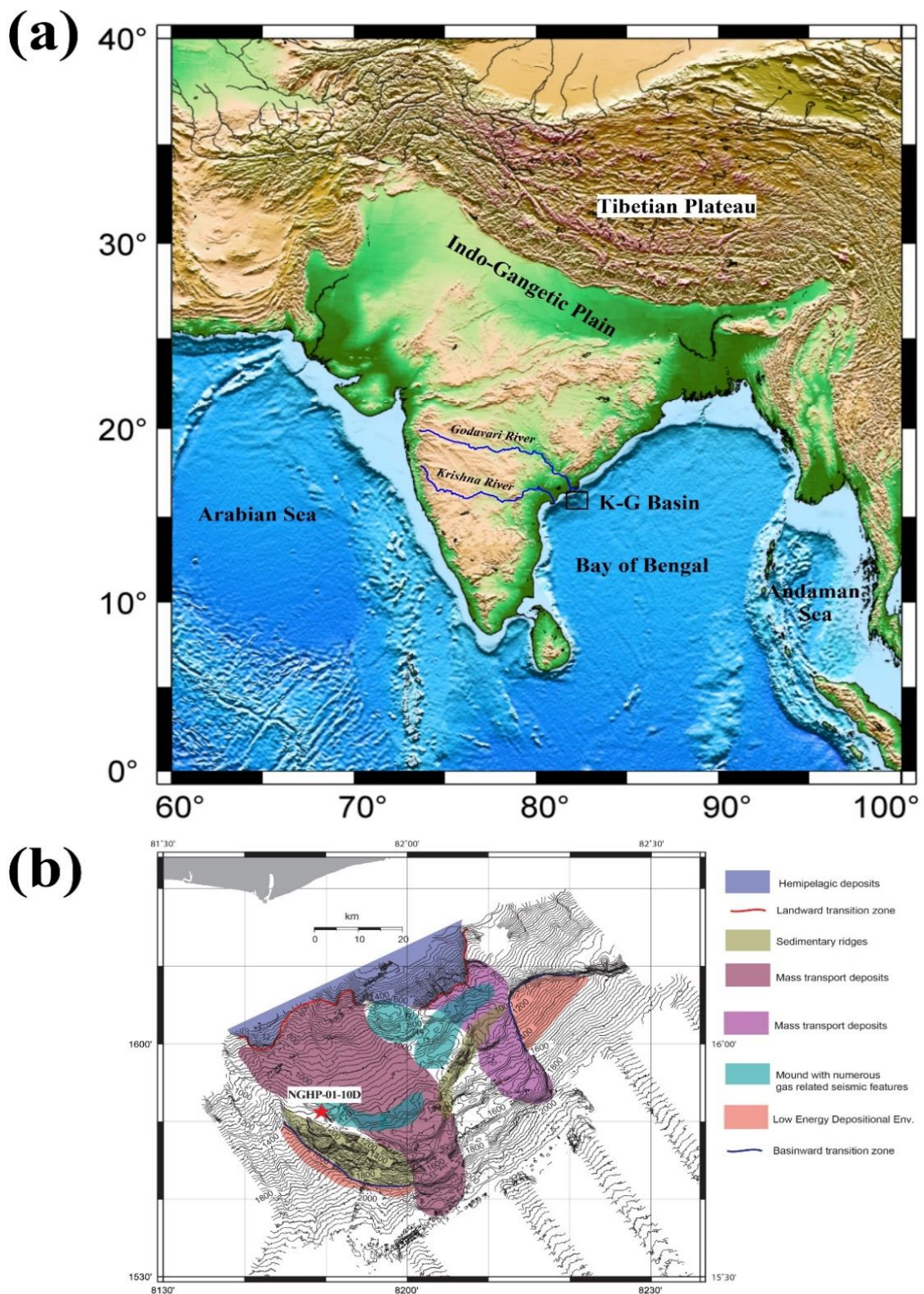


**Figure 1.** (a) Map showing the location of KG-basin on the eastern continental shelf of India. (b) Bathymetric map of the study area in the KG-basin (modified after Dewangan et al., 2010). The red star in the map indicates the location of the NGHP-01-10D sediment core site.

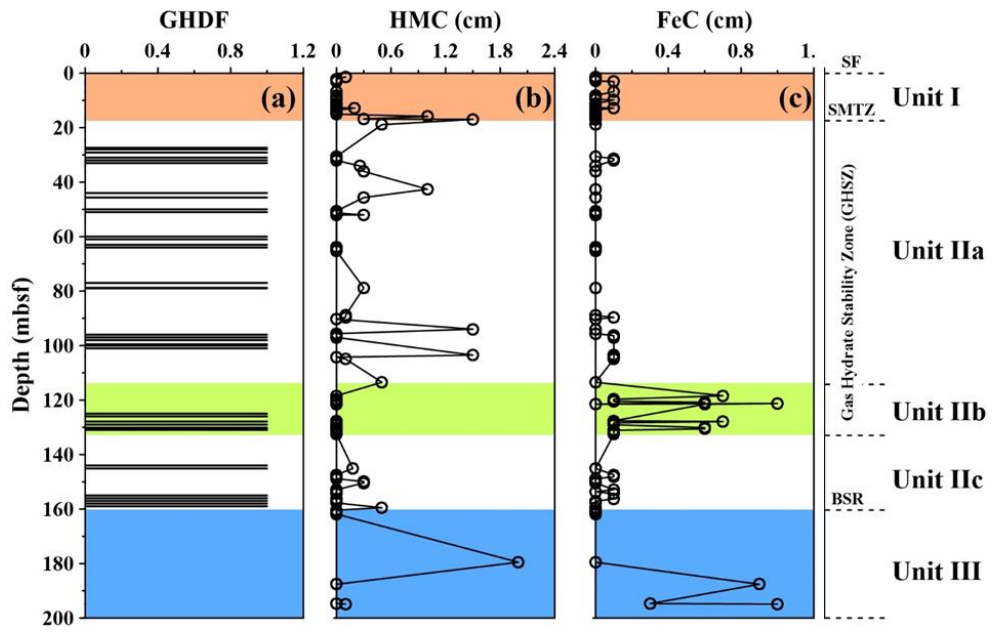


**Figure 2.** Down-core distributions of (A) mousey/soupy sediment layers representing gas-hydrate dissociation features; (B) sizes of High-Mg carbonate (HMC) concretions; and (C) sizes of Fe-rich carbonates concretions (FeC).

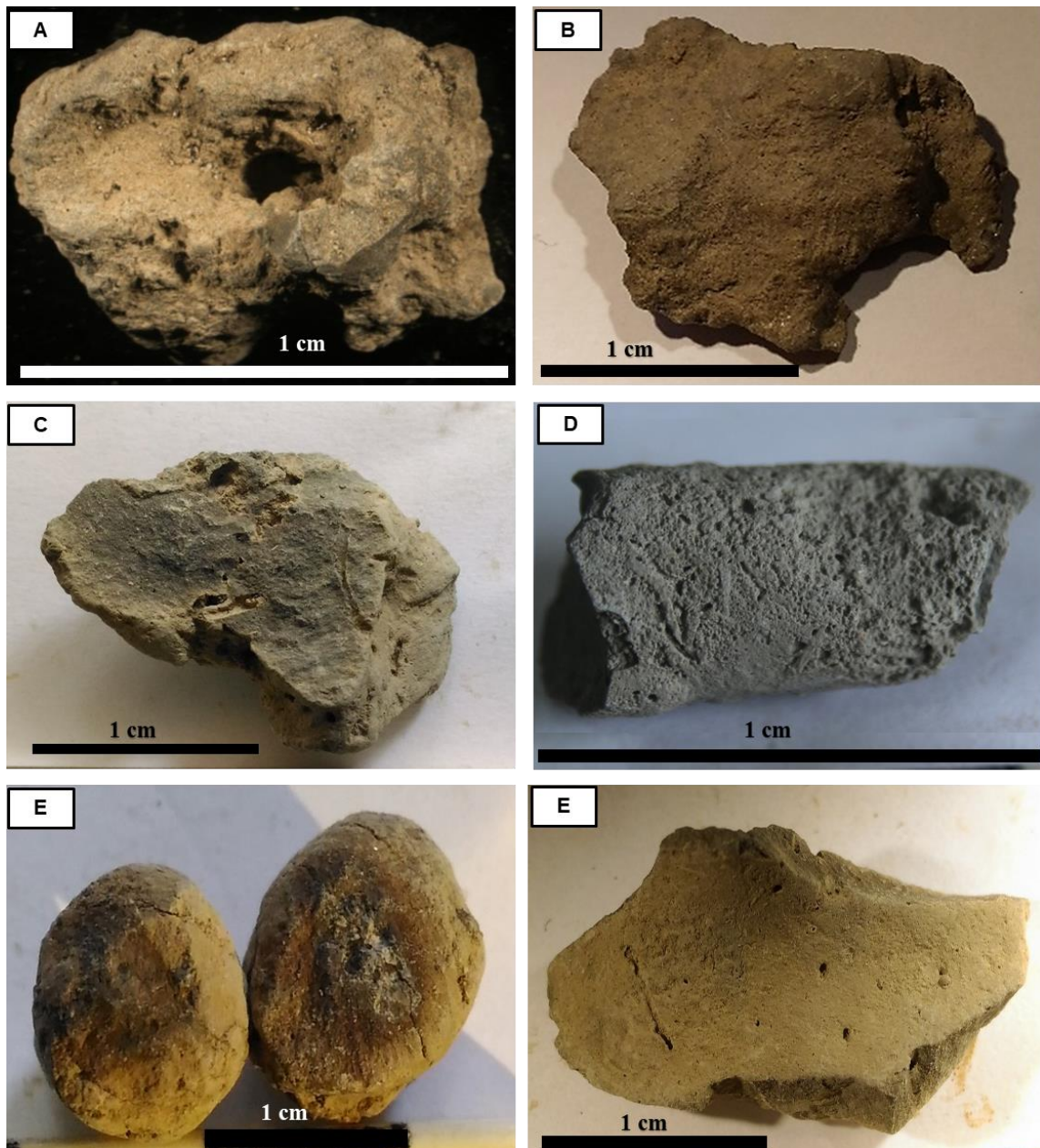


**Figure 3.** *Morphology of authigenic carbonates. (A-B) Lithified High-Mg calcite (HMC) nodules exhibiting surface characteristics indicative of gas escape features; (C-D) Highly lithified High-Mg calcite; (E-F) semi-lithified siderite nodules. The scale bar in each photograph represents 1.0cm.*

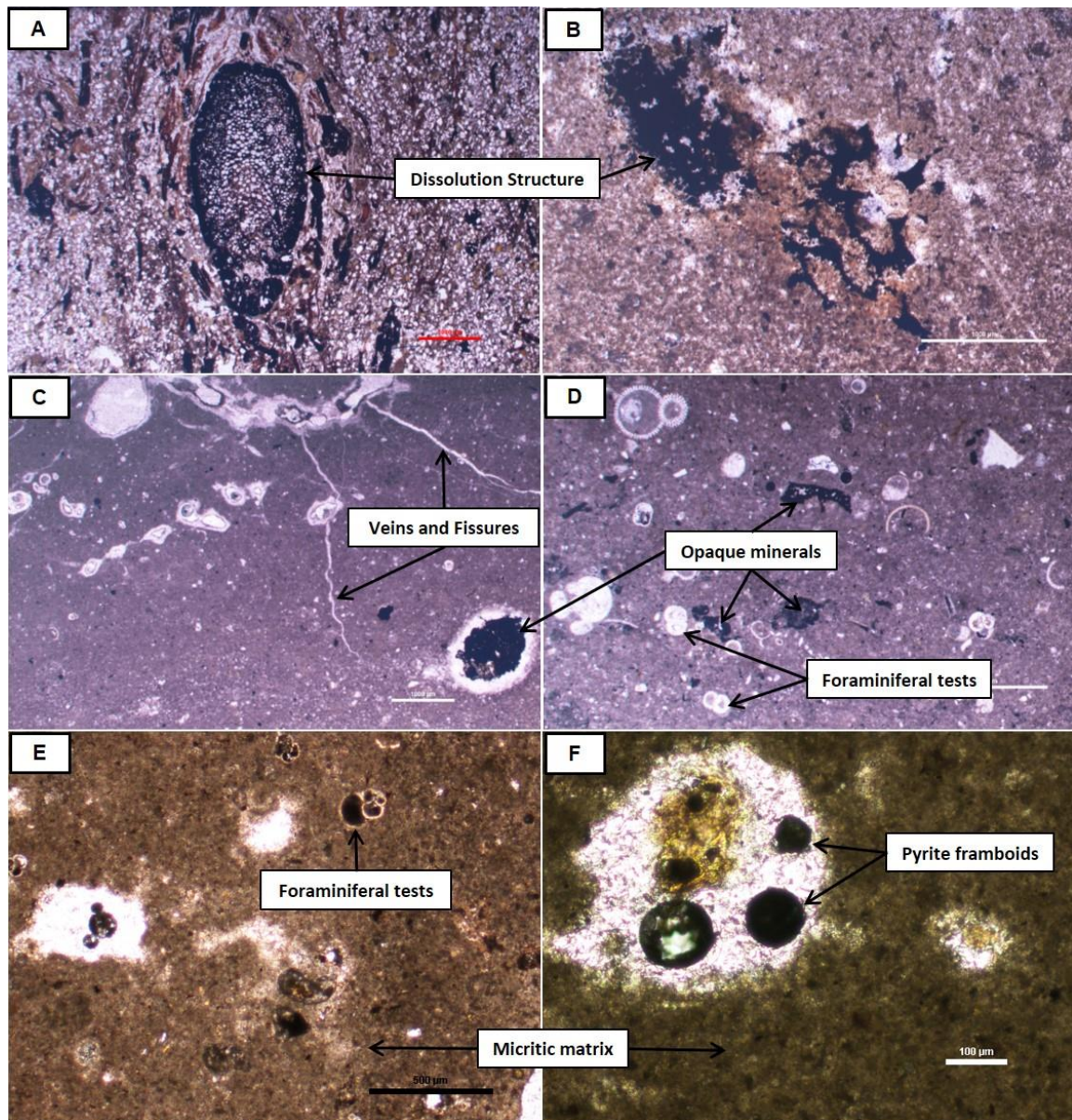


**Figure 4.** Photomicrographs of authigenic carbonates-showing (A-D) High-Mg calcites and (E&F) siderite. (A&B) Inter-crystalline pores representing the dissolution structures in HMC concretions; (C&D) Micritic matrix of HMC with veins and fissures; and foraminiferal tests; (E&F) Micritic texture of siderite with foraminiferal tests filled with pyrite framboids.



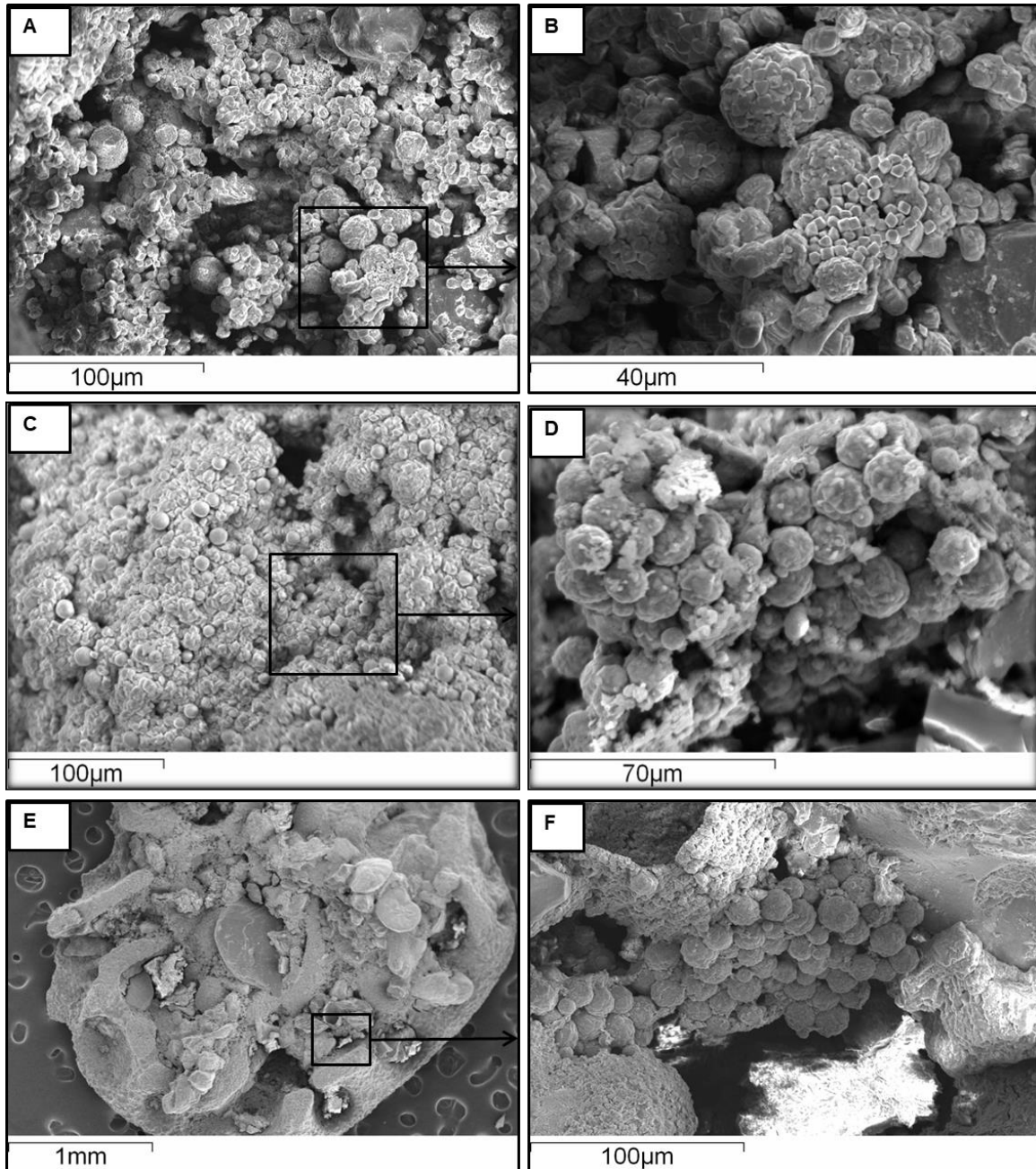


**Figure 5.** SEM micrographs of authigenic carbonates. (A-D) Cluster of pyrite framboids; (E&F) Thin slab of siderite (Fe-carbonate) in which pyrite framboids are seen along with gypsum and forams.

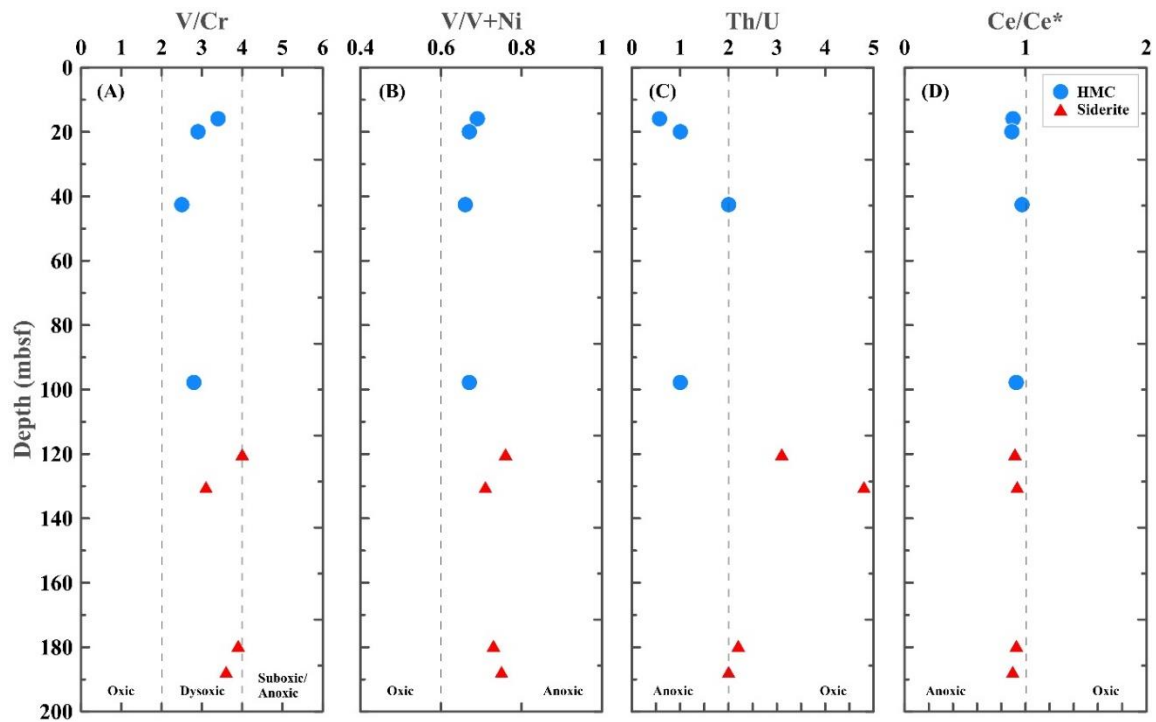


**Figure 6.** Down core distributions of paleo-redox indices like (A) V/Cr, (B) V/V+Ni, (C) Th/U and (D) Ce/Ce\* ratios in HMC and siderites show mostly oxygen-depleted environments persisted during the authigenic carbonate formation at site in NGHP-01-10D. The optimum values of the elemental indices corresponding to different redox regimes are obtained from Jones and Mannings, 1994; Wignall and Twitchett, 1996.

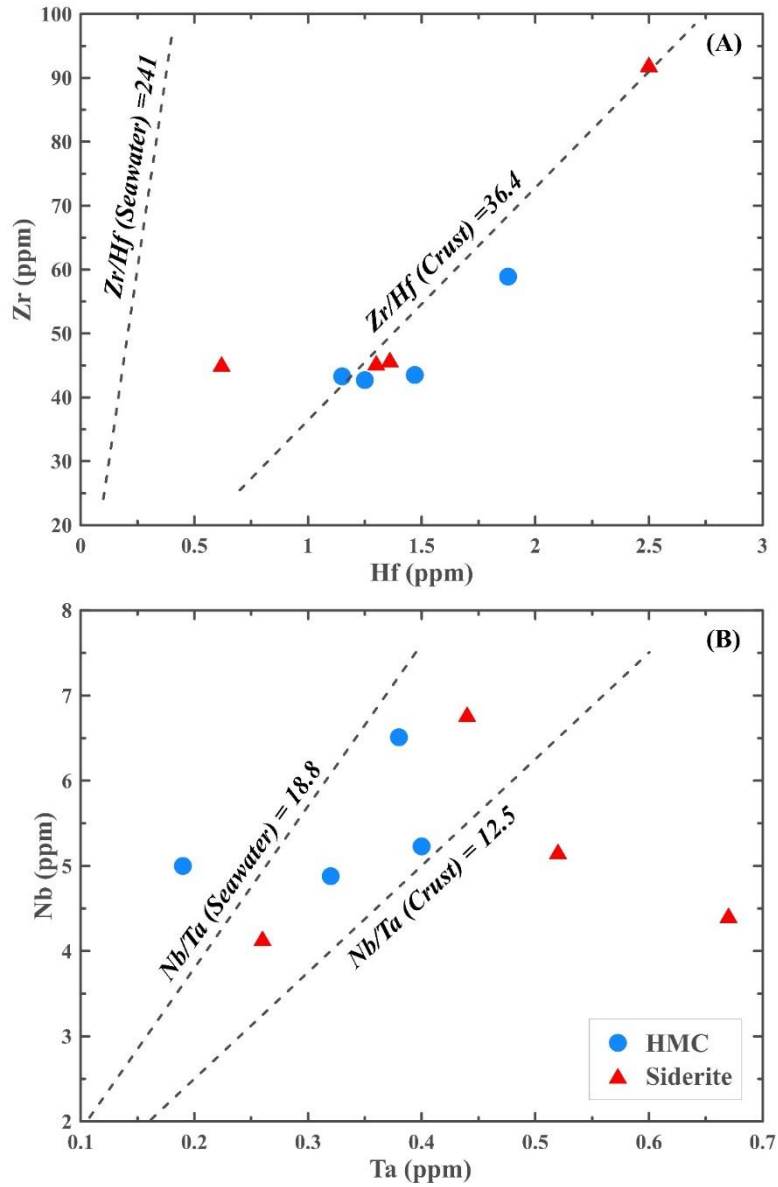


**Figure 7.** Bivariate plots of Zr vs. Hf (A) and Nb vs. Ta (B) in HMC and siderites from NGHP-01-10D core: dotted lines are corresponding average compositions of deep seawater (Firdaus *et al.*, 2011) and upper crusts (David *et al.*, 2000; Barth *et al.*, 2000).

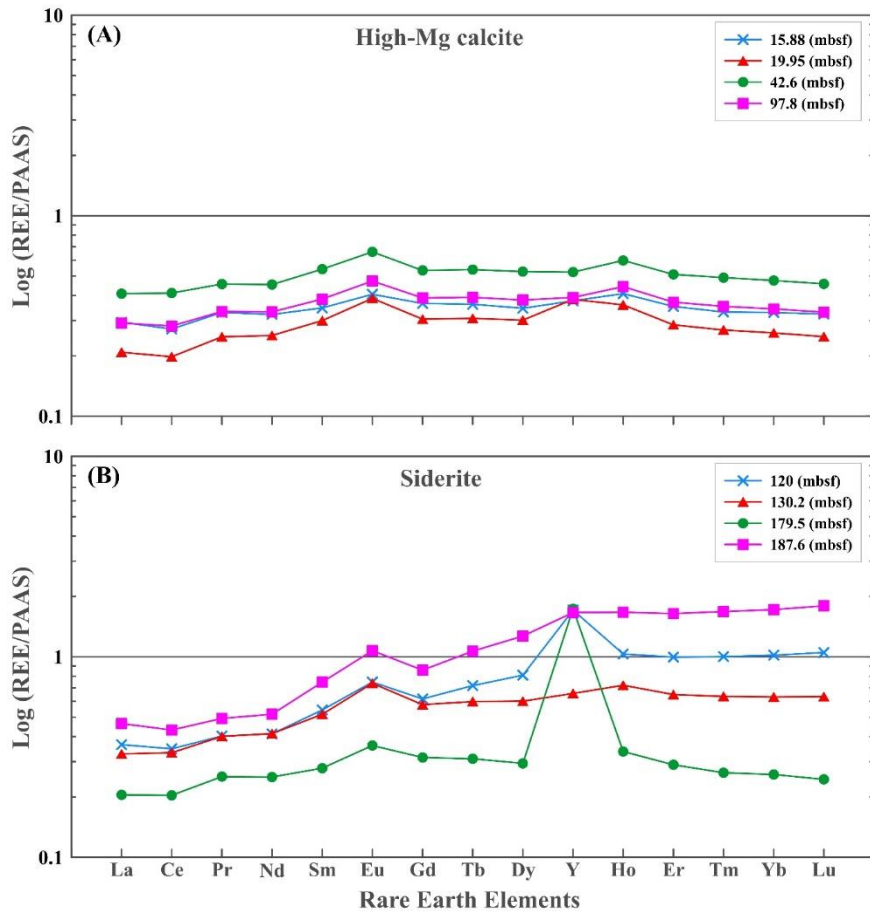


**Figure 8.** Post Archean Australian Shale (PAAS) normalized REE-Y patterns of the (A) High-Mg calcite concretions and (B) siderite concretions separated from sediments at different depths of the NGHP-01-10D core. PAAS Normalization values are from Taylor and McLennan (1985).

**Tables:****Table 1.** *Physical nature, mineralogy, total inorganic carbon, and C-isotopic composition of dominant authigenic carbonates from different depths of the core, NGHP-01-10D.*

<b>Sample depth (mbsf)</b>	<b>Color &amp; degree of Lithification</b>	<b>Morphology of carbonate concretion</b>	<b>Dominant carbonate</b>	<b>TIC (wt%)</b>	<b><math>\delta^{13}\text{C}</math> (‰PDB)</b>	<b><math>\delta^{18}\text{O}</math> (‰PDB)</b>
<b>15.88</b>	Grayish & Soft	Nodule	High-Mg Calcite	8.75	-45.75	4.81
<b>19.95</b>	Grayish & Soft	Nodule	High-Mg Calcite	9.23	-50.28	4.31
<b>42.61</b>	Grayish & Soft	Nodule	High-Mg Calcite	9.10	-45.6	4.26
<b>97.8</b>	Grayish & Soft	Nodule	High-Mg Calcite	9.22	-52.4	4.61
<b>120.0</b>	Brownish & Hard	Nodule	Siderite	9.20	+9.86	4.26
<b>130.2</b>	Brownish & Soft	Nodule	Siderite	7.98	+9.76	4.37
<b>179.5</b>	Brownish & Hard	Nodule	Siderite	NA	NA	4.23
<b>187.6</b>	Brownish & Hard	Nodule	Siderite	7.76	+4.92	4.13

*\*NA= Not analyzed*

**Table 2.** Analytical data of major oxides (wt%) in High-Mg calcites (HMCs) and siderites at different depths of the sediment core, NGHP-01-10D.

Major element	HMC				Siderite			
	15.88 (mbsf)	19.95 (mbsf)	42.6 (mbsf)	97.8 (mbsf)	120 (mbsf)	130.2 (mbsf)	179.5 (mbsf)	187.6 (mbsf)
<b>SiO<sub>2</sub></b>	12.3	12.2	10.7	11.5	7.0	8.8	4.85	8.90
<b>Al<sub>2</sub>O<sub>3</sub></b>	3.38	3.26	2.86	2.91	1.71	2.18	0.85	2.32
<b>TiO<sub>2</sub></b>	0.26	0.27	0.21	0.25	0.31	0.41	0.18	0.37
<b>Fe<sub>2</sub>O<sub>3</sub></b>	2.29	2.38	2.33	2.08	43.7	42.0	48.7	38.5
<b>MnO</b>	0.02	0.15	0.02	0.02	0.29	0.56	0.02	0.3
<b>MgO</b>	6.05	5.03	5.44	5.26	3.52	3.31	0.79	6.0
<b>CaO</b>	39.5	39.3	39.6	39.2	4.38	6.14	1.24	7.27
<b>Na<sub>2</sub>O</b>	0.19	0.23	0.19	0.14	0.25	0.27	0.22	0.2
<b>K<sub>2</sub>O</b>	0.69	0.63	0.52	0.66	0.44	0.51	0.24	0.39
<b>P<sub>2</sub>O<sub>5</sub></b>	0.18	0.33	0.19	0.12	0.41	0.44	0.07	0.49
<b>MgO/CaO</b>	0.15	0.13	0.14	0.13	0.80	0.54	0.64	0.83

**Table 3.** Concentrations of trace elements (ppm) in HMC and siderites at different depths in the core NGHP-01-10D.

Trace elements	HMC				Siderite			
	15.88 (mbsf)	19.95 (mbsf)	42.6 (mbsf)	97.8 (mbsf)	120 (mbsf)	130.2 (mbsf)	179.5 (mbsf)	187.6 (mbsf)
<b>Sc</b>	7.58	7.48	8.52	7.72	7.31	9.58	8.06	9.54
<b>V</b>	61.3	56.1	64.4	56.4	61.9	75.1	62.7	65.2
<b>Cr</b>	17.8	19.6	26.1	19.9	15.5	24.1	16.2	18.3
<b>Co</b>	7.27	7.93	10.5	8.16	3.8	11.8	4.5	6.0
<b>Ni</b>	26.8	27.7	32.0	27.9	19.7	29.9	22.5	21.5
<b>Cu</b>	11.8	14.8	18.3	15.0	14.7	16.4	15.4	14.4
<b>Zn</b>	27.7	26.5	31.4	26.7	20.5	22.8	21.2	20.7
<b>Ga</b>	8.22	8.83	11.8	9.06	7.79	12.6	8.54	8.52
<b>Rb</b>	19.6	19.6	24.2	19.8	13.7	18.0	14.4	13.9
<b>Sr</b>	954	1015	1132	1010	227	669	228	227
<b>Cs</b>	0.94	0.73	1.01	0.96	0.53	0.67	0.71	0.60
<b>Ba</b>	110	112	135	119	114	202	116	115
<b>Zr</b>	42.7	43.3	58.9	43.5	45.2	92.1	45.9	45.4
<b>Nb</b>	4.88	5.00	6.51	5.23	4.42	6.78	5.17	4.15
<b>Hf</b>	1.25	1.15	1.88	1.47	0.62	2.50	1.36	1.30
<b>Ta</b>	0.32	0.19	0.38	0.40	0.67	0.44	0.52	0.26
<b>Pb</b>	16.6	13.4	13.3	13.6	12.2	13.6	12.9	11.9
<b>Th</b>	3.30	3.48	5.32	3.71	3.42	4.47	4.16	3.64
<b>U</b>	5.74	3.48	2.47	3.71	1.09	0.93	1.84	1.82
<b>V/Cr</b>	3.4	2.9	2.5	2.8	4.0	3.1	3.9	3.6
<b>V/V+Ni</b>	0.69	0.67	0.66	0.67	0.76	0.71	0.73	0.75
<b>Th/U</b>	0.57	1.0	2.0	1.0	3.1	4.8	2.2	2.0
<b>Sr/Ba</b>	8.7	9.1	8.4	8.5	2.0	3.3	1.9	2.0
<b>Zr/Hf</b>	34.2	37.7	31.3	29.6	72.9	36.8	33.7	34.9
<b>Nb/Ta</b>	15.2	26.3	17.1	13.1	6.6	15.4	9.9	16.0

*V/Cr* < 2 (Oxic); 2-4.25 (dysoxic); > 4.25 (suboxic to anoxic).

*V/V+Ni* < 0.6 (dysoxic); 0.6-0.84 (suboxic); > 0.84 (euxinic).

*U/Th* < 0.75 (Oxic); 0.75-1.25 (Dysoxic); > 1.25 (anoxic).

**Table 4.** Concentrations of REE and Y (ppm) in HMC and siderites at different depths of the core, NGHP-01-10D.

Rare earth elements	HMC				Siderite			
	15.88 (mbsf)	19.95 (mbsf)	42.6 (mbsf)	97.8 (mbsf)	120 (mbsf)	130.2 (mbsf)	179.5 (mbsf)	187.6 (mbsf)
<b>La</b>	11.19	7.92	15.52	11.09	13.86	12.46	7.79	17.66
<b>Ce</b>	21.66	15.76	32.74	22.43	27.68	26.46	16.23	34.33
<b>Pr</b>	2.91	2.20	4.03	2.94	3.56	3.54	2.23	4.35
<b>Nd</b>	10.91	8.57	15.37	11.23	13.99	14.04	8.53	17.54
<b>Sm</b>	1.93	1.66	3.01	2.13	3.02	2.87	1.55	4.15
<b>Eu</b>	0.44	0.42	0.71	0.51	0.81	0.80	0.39	1.16
<b>Gd</b>	1.70	1.42	2.49	1.81	2.87	2.69	1.47	4.00
<b>Tb</b>	0.28	0.24	0.42	0.30	0.56	0.46	0.24	0.83
<b>Dy</b>	1.62	1.41	2.46	1.78	3.79	2.81	1.38	5.94
<b>Y</b>	10.16	10.33	14.13	10.56	46.16	17.73	46.9	44.89
<b>Ho</b>	0.41	0.36	0.59	0.44	1.02	0.72	0.33	1.65
<b>Er</b>	1.01	0.81	1.45	1.06	2.84	1.85	0.83	4.68
<b>Tm</b>	0.13	0.11	0.20	0.14	0.41	0.26	0.11	0.68
<b>Yb</b>	0.93	0.73	1.34	0.97	2.87	1.78	0.73	4.85
<b>Lu</b>	0.14	0.11	0.20	0.14	0.46	0.27	0.11	0.78
<b>∑REE</b>	<b>55.2</b>	<b>41.7</b>	<b>80.5</b>	<b>57.0</b>	<b>77.7</b>	<b>71.0</b>	<b>41.9</b>	<b>102.6</b>
<b>Nd<sub>n</sub>/Yb<sub>n</sub></b>	0.98	0.39	0.97	0.95	0.97	0.41	0.66	0.97
<b>Eu/Eu*</b>	1.14	1.31	1.28	1.23	1.22	1.29	1.35	1.22
<b>Ce/Ce*</b>	0.90	0.90	0.89	0.96	0.92	0.91	0.93	0.93
<b>Y/Ho</b>	24.7	28.7	23.9	24.0	45.2	24.6	142.1	27.2

\*Cerium anomaly,  $Ce/Ce^* = 3Ce_n / (2La_n + Nd_n)$  & Eu anomaly,  $Eu/Eu^* = 3Eu_n / (2Sm_n + Tb_n)$